Experimental and Numerical Studies on Buckling and Post-Buckling Behavior of Cylindrical Panels Subjected to Compressive Axial Load

M. Shariati, J. Saemi, M. Sedighi, and H. R. Eipakchi

Shahroud University of Technology, Shahroud, Iran

Экспериментальное исследование и численное моделирование потери устойчивости цилиндрических панелей при сжатии осевой нагрузкой

М. Шариати, Дж. Саеми, М. Седиги, Х. Р. Эйпакчи

Технологический университет г. Шахруд, Иран

С использованием экспериментальных и численных расчетных методик исследовано поведение цилиндрических панелей после потери устойчивости. Проанализировано влияние длины, угловых параметров секторов и различных граничных условий цилиндрических панелей на величину нагрузки, при которой происходит потеря устойчивости. Экспериментальные исследования проводились на сервогидравлической испытательной машине Instron 8808, для расчетов использовался конечноэлементный пакет программ Abaqus. Получено хорошее соответствие расчетных результатов с экспериментальными.

Ключевые слова: механические испытания, упругопластическое деформирование, анализ потери устойчивости.

Introduction. Shell structures are widely used in pipelines, aerospace and marine structures, large dams, shell roofs, liquid-retaining structures and cooling towers [1]. Buckling is one of the main failure considerations when designing these structures [2]. At first, researchers focused on the determination of the buckling load in the linear elastic zone, but experimental studies [3, 4] showed that the buckling capacity of thin cylindrical shells is much lower than that predicted by classic theories [5]. Thin cylindrical panels are used in different structures. When the stress distribution in this structure is compressive, the structure will collapse usually before yielding or the buckling phenomena determines its loading capacity due to large value of radius to thickness ratio. This subject is usually studied using the numerical methods based on the finite elements (FE) and analytical methods in elastic region. The exact solution for isotropic and anisotropic panels has been presented by Timoshenko [6] and Lekhnitskii [7]. El-Raheb [8] investigated the stability of simply supported panels subjected to uniform external pressure. Magnucki et al. [9] solved the Donnell equation for buckling of panels with three simply supported edges and one free edge subjected to axial load using the Galerkin method. Patel et al. [10] discussed static and dynamic stability of panels with edge harmonic loading. Buermann et al. [11] presented a semi-analytical

model for the post-buckling analysis of stiffened cylindrical panels using trigonometric Fourier series as approximated solutions for displacements. Lanzi et al. [12] performed a multi-objective optimization procedure based on Genetic Algorithms for the design of composite stiffened panels capable to operate in post-buckling conditions. The results without considering any kind of imperfection, are closed and in good agreement with the tests in terms of buckling and post-buckling stiffness, as well as of collapse loads. Jiang et al. [13] studied the buckling of panels subjected to compressive stress using the differential quardrature element method. Keweon [14, 15] carried out numerical and experimental studies of the post-buckling behavior of axially loaded cylindrical panel with clamped curved edges and with simply supported straight edges. Bisagni et al. [16] presented an analytical formulation for the study of linearized local skin buckling load and nonlinear post-buckling behavior of isotropic and composite stiffened panels subjected to axial compression. The results are compared with the FE analysis.

In this paper, numerical and experimental studies have been performed on cylindrical panels for determining the buckling load and investigating the post-buckling behavior of panels. For numerical analysis Abaqus FE package has been used to study the effects of the length, sector angle, thickness and different boundary conditions and the experimental tests have been applied to the panels using a servo-hydraulic machine. The experimental results are in good agreement with the experimental ones.

1. **Panels Characteristics**. Figure 1 shows the schematic of a panel. The mechanical properties of metal panels have been determined using tensile tests. For this purpose, some standard test specimens have been prepared from the original tubes according to ASTM E8 [17] standard and tensile tests were performed using an Instron 8802 tensile test machine.

Figure 2 shows the stress–strain diagram for a specimen. Poisson's ratio was assumed to be 0.33. The geometrical and mechanical properties of panels are listed in Table 1.
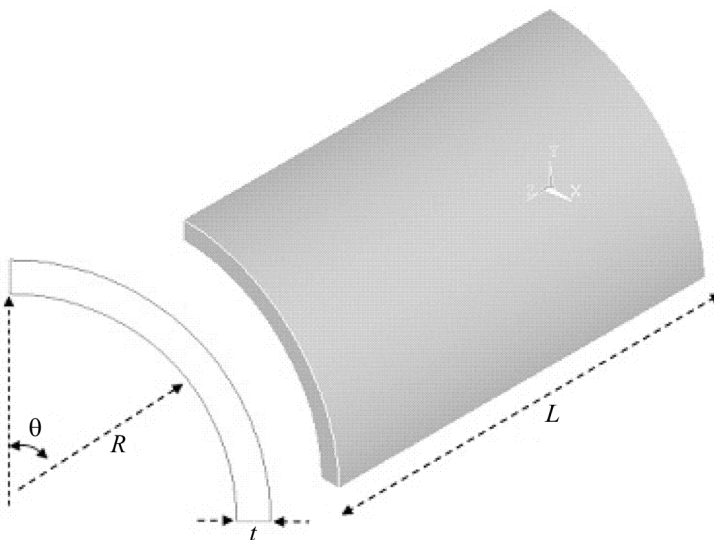

Fig. 1. Schematic of a cylindrical panel.

T a b l e 1

Mechanical and Geometrical Properties of Panels

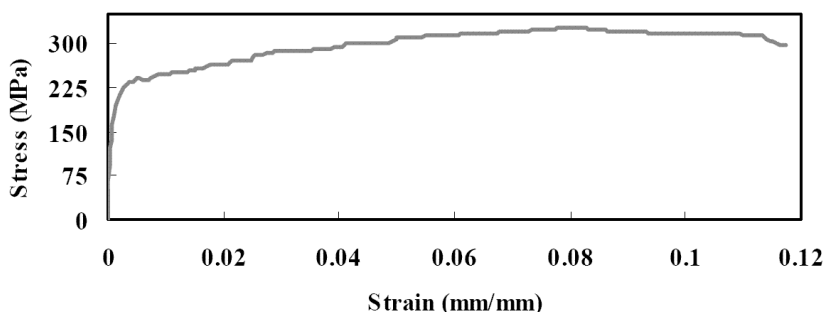| Outer diameter D, mm	60
Thickness t, mm	0.9
Sector angle θ, deg	90, 120, 180, 355, and 360 (perfect)
Length L, mm	100, 150, and 250
Yield stress σ_Y, MPa	240
Young modulus E, GPa	150
Poisson's ratio	0.33

Fig. 2. Stress–strain diagram.

2. **Boundary Conditions**. For applying boundary conditions at the edges of the cylindrical panel, two rigid plates were used that were attached to the edges of the cylindrical panel. In order to analyze the buckling under axial loading similar to the experimental conditions, a 15-mm displacement was applied to the center of the upper plate, which resulted in a distributed compressive load on both edges of the cylindrical panel. Additionally, all degrees of freedom in the lower plate and upper plate, except in the direction of longitudinal axis, were constrained.

In the section of experimental results, it will be shown that the fulcrum used in these tests has an edge that is 18.1 mm high (Fig. 3). For this reason, in numerical simulations, the edges of the shell are constrained to this elevation, except in the direction of the cylinder axis.
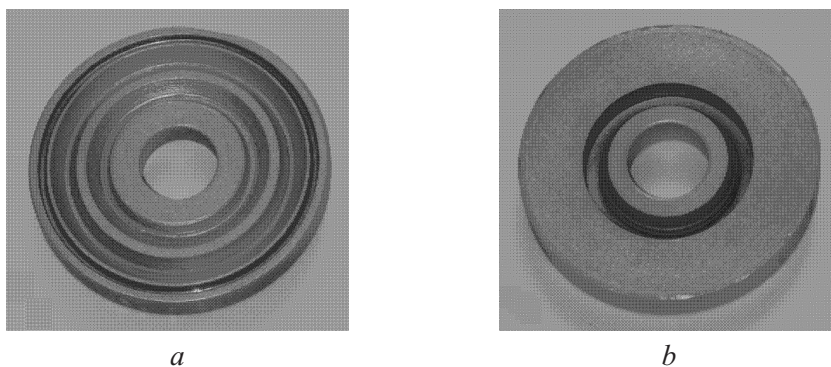

Fig. 3. Fixtures for experimental test: (*a*) simply supported; (*b*) clamped.

3. **Numerical Method**. The numerical analysis has been performed with Abaqus FE package. For this analysis, the nonlinear element S8R5 (which is an eight-node element with six degrees of freedom per node, suitable for analysis of thin shells) and the linear element S4R (which is a four-node element) were used [18]. Part of a meshed specimen is shown in Fig. 4. Both linear and nonlinear elements were used for the analysis of the shells and the results were compared with each other.
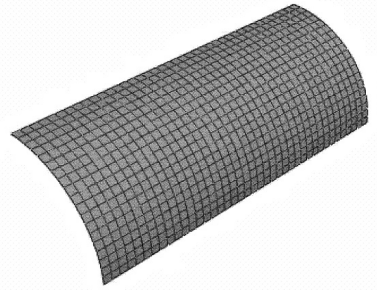

Fig. 4. Mesh pattern for a panel.

The boundary conditions under study were clamped or simple (at arc edges) and free (at straight edges). Eigenvalue analysis overestimates the value of buckling load, because in this analysis the plastic properties of material play no role in the analysis procedure. For buckling analysis, an eigenvalue analysis should be perfomed initially for all specimens, to find the mode shapes and corresponding eigenvalues. Primary modes have smaller eigenvalues and buckling usually occurs in these mode shapes. For eigenvalues analysis the "Buckle step" was used in the software. Three initial mode shapes and corresponding displacements of all specimens were obtained. The effects of these mode shapes must be considered in nonlinear buckling analysis ("Static Riks" step). Otherwise, the software would choose the buckling mode in an arbitrary manner, resulting in unrealistic results of nonlinear analysis. For "Buckle step", the subspace solver method of the software was used. It is noteworthy that, due to the presence of contact constraints between rigid plates and the shell, the Lanczos solver method cannot be used for these specimens [18]. In Fig. 5, two primary mode shapes are shown for the specimen with $L = 100$ mm, $\theta = 90°$. After completion of the buckle analysis, a nonlinear analysis was performed to plot the load–displacement curve. The maximum value attained by this curve is the buckling load.
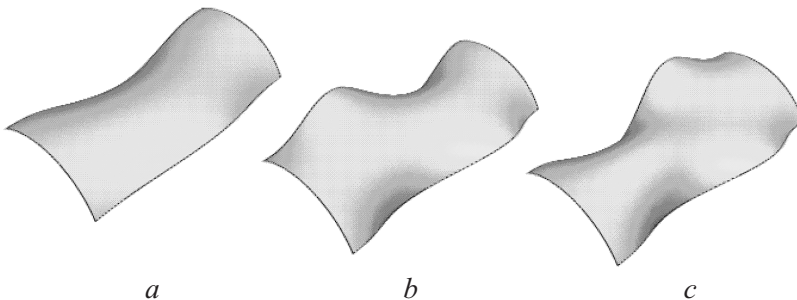

a   *b*   *c*

Fig. 5. Buckling mode shape for specimen with $L = 100$ mm, $\theta = 90°$: (*a*) first mode, (*b*) second mode, and (*c*) third mode.

This step, called "Static Riks" involves the arc length method for post-buckling analysis. In this analysis, nonlinearity of both material properties and geometry is taken into consideration. This analysis has been performed for different panels (Table 1) for clamped and simple boundary conditions, and the load–displacement diagram has been derived for each case.

4. **Experimental Method**. Some specimens with characteristics listed in Table 1 were prepared and the compression test of panels was performed using a servo-hydraulic machine. At first, for investigating the system reliability for repeating the tests, three similar panels with $L = 100$ mm and $\theta = 120°$ were tested. Figure 6 shows the load–displacement diagrams for these panels, which indicates repeatability of the panel tests.
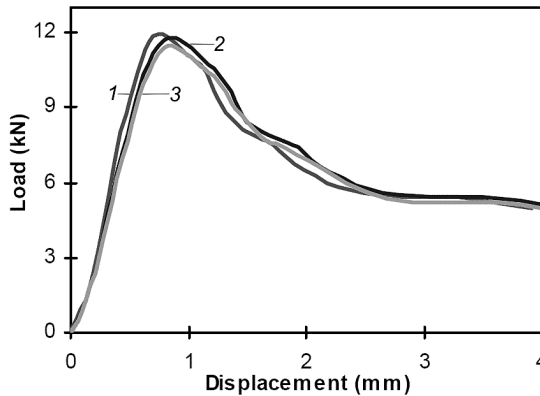
Fig. 6. Load–displacement diagrams for three similar panels with $L = 100$ mm, $\theta = 120°$: (*1*) test 1, (*2*) test 2, and (*3*) test 3.

For different boundary conditions, the axial load was applied to the panels and the load–axial displacement diagrams of panels have been drawn.

In all tests, the straight edges were free and the arc edges were clamped or simply supported. To produce clamped and simple boundary conditions, some appropriate fixtures were designed. Figure 7 shows the test setup.
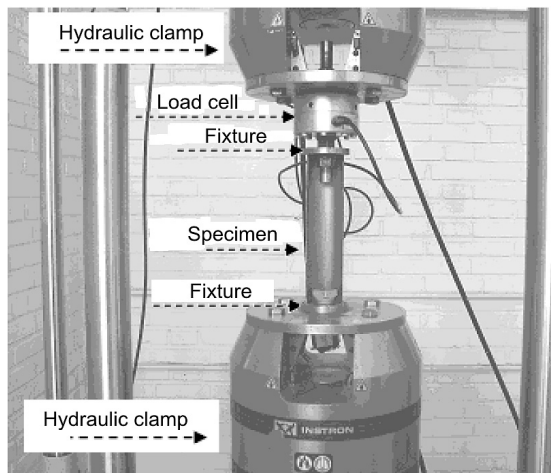

Fig. 7. Experimental test setup.

5. **Discussion of Results**. Figure 8 shows the numerical and experimental load–displacement diagrams for panels of different lengths. The peak values in diagrams stand for the buckling load. It is seen that with increase in the length the buckling load decreases. These variations are more pronounced for smaller lengths. For higher lengths, the load–displacement diagram for the smallest sector angle, i.e., $\theta = 90°$ (Fig. 9) tends to the Euler buckling mode.
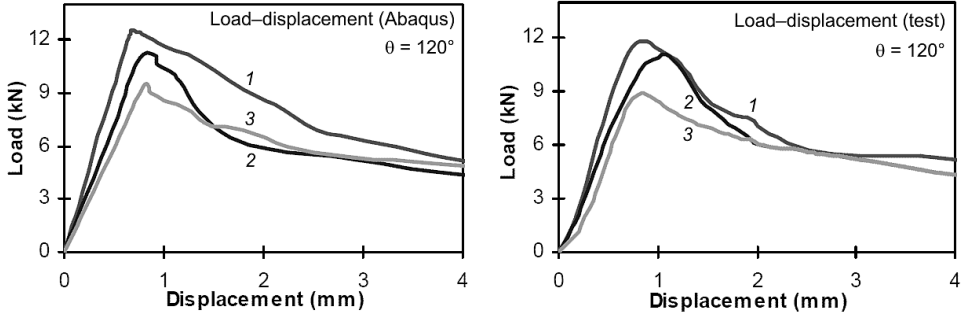

Fig. 8. Load–displacement diagrams for different lengths ($\theta = 120°$, simply supported). [Here and in Figs. 9 and 10: (*1*) $L = 100$ mm; (*2*) $L = 150$ mm; (*3*) $L = 250$ mm.]

Figures 9 and 10 show the load–displacement diagrams for $\theta = 90$ and $180°$.

Figure 11 shows that with increase in the sector angle the buckling load increases. When there is a narrow cut ($\theta = 355°$), the buckling load drops noticeably. The variations of the buckling load in terms of the sector angle (shown in Fig. 12) are nearly linear and change considerably for a cylinder. Figure 13 shows the deformed shape of a panel with a narrow cut.
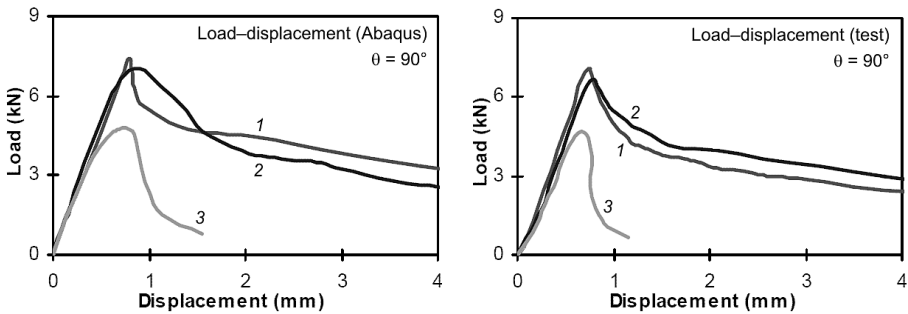
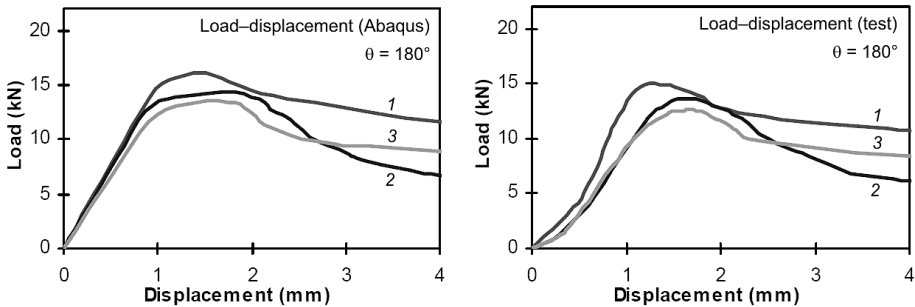Fig. 9. Load–displacement diagrams for different lengths ($\theta = 90°$, simply supported).

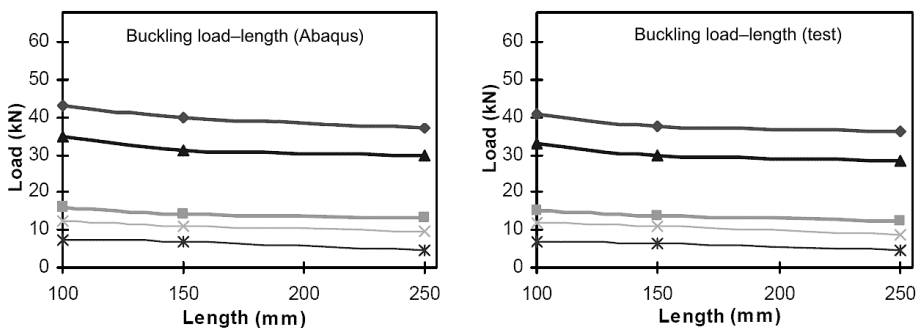Fig. 10. Load–displacement diagram for different lengths ($\theta = 180°$, simply supported).

Fig. 11. Buckling load in terms of the length for different sector angles: ($\blacklozenge$) perfect; ($\blacktriangle$) $\theta = 355°$; ($\blacksquare$) $\theta = 180°$; ($\times$) $\theta = 120°$; ($\ast$) $\theta = 90°$.
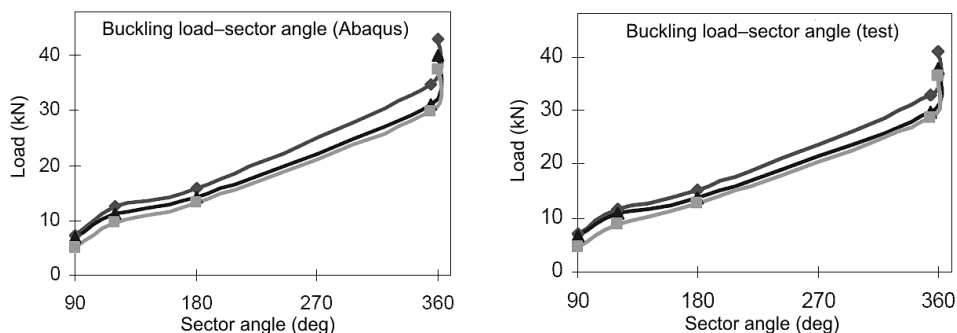

Fig. 12. Buckling load in terms of the sector angle for different sector angles (simply supported): ($\blacklozenge$) $L = 100$ mm; ($\blacktriangle$) $L = 150$ mm; ($\blacksquare$) $L = 250$ mm.

a b
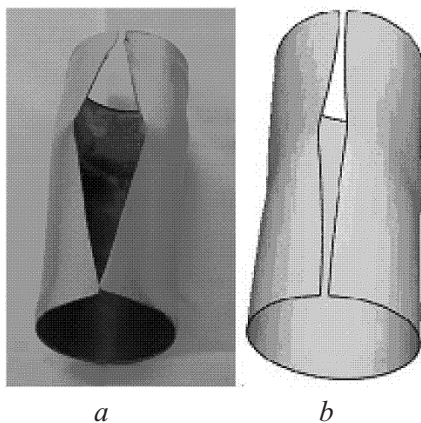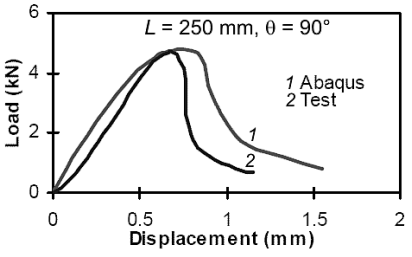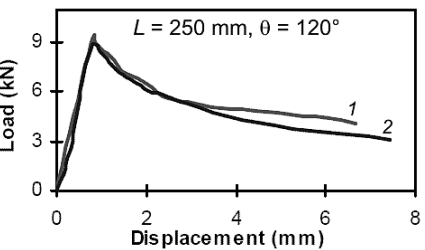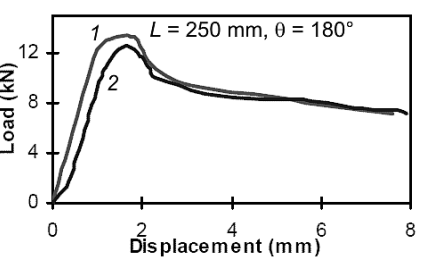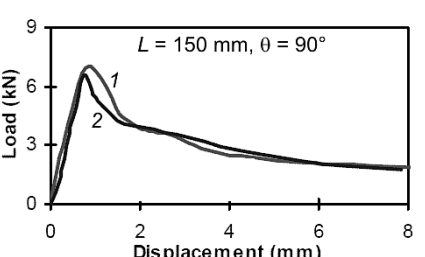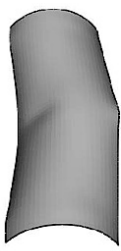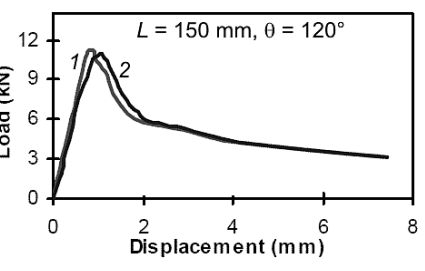
Fig 13. Deformed shaped of panel ($\theta = 355°$, $L = 100$ mm, simply supported): (*a*) experimental; (*b*) numerical.

The load–displacement diagrams and the first buckling modes for different panels are shown in Table 2. The buckling modes are similar and there is a good agreement between the load–displacement diagrams in the most cases.

The largest differences between the diagrams correspond to the post-buckling region and the values for FE results are higher than the experimental values. It may be due to approximated definition of the plastic part of stress–strain diagram and no consideration of the specimens defects in FE model. The FE stress analysis

T a b l e 2
**Numerical and Experimental Load–Displacement Diagrams and Buckling Modes
for Different Lengths and Sector Angles**

Numerical mode	Experimental mode	Load–displacement diagram
1	2	3

shows that in some cases, the von Mises stresses in panels are higher than the yield stress or the panel is not elastic at buckling load. Figure 14 shows the von Mises stresses of a panel under buckling load.

5.1. *Effect of Boundary Conditions*. To investigate the effects of different boundary conditions, some tests were performed on panels with clamped and simple supports. Table 3 shows the load–displacement diagrams for clamped and simply supported boundary conditions. Results show that in all tests the clamped boundary conditions can increase the buckling load capacity of the panels. This is due to the fact that clamped boundaries can restrict the number of degrees of freedom. The Euler buckling mode has been observed for $L = 250$ mm and $\theta = 90°$ in numerical and experimental results. The values of buckling loads for these boundary conditions are listed in Table 4.
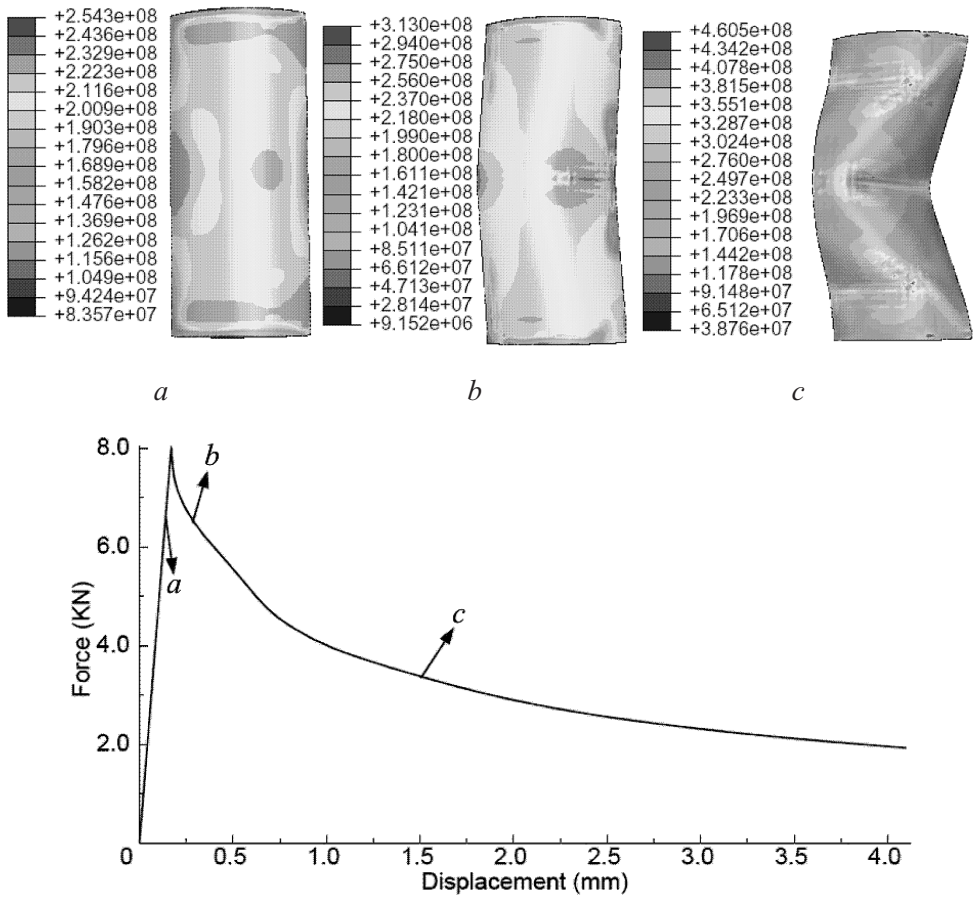
Fig. 14. Von Mises stress distribution in panel due to different loads (simply supported): (*a*) applied load is in the elastic region; (*b*, *c*) applied loads are in the post-buckling region.

5.2. *Effect of Linear and Nonlinear Elements*. After comparing the curves in Fig. 15, it can be noted that linear elements, in contrast to nonlinear elements, have a better prediction power for the post-buckling behavior of mild steel cylindrical shells with elliptical cutouts. In the prebuckling phase, both elements produce similar results.

It can be seen that the slope of load vs. displacement curves prior to the buckling is higher in numerical results than in the experimental ones. This discrepancy is due to the presence of internal defects in the material which reduces the stiffness of the specimens in the experimental method, while the materials are assumed to be ideal in the numerical analysis.

The experimental results are compared with numerical findings in Table 5. It is evident that there is a close correlation between experimental and numerical results. For example, the biggest discrepancy between the two sets of results is 6.7% for S8R5 nonlinear element and 8.8% for S4R linear element. It is also noteworthy that the greatest difference is observed for short specimens. This can be attributed to the fact that the bending theory of shells is more suitable for lower t/L ratios, while and this theory is used by the software for calculations.

T a b l e 3

Load–Displacement Diagrams for Clamped and Simply Supported Boundary Conditions

Numerical	Experimental
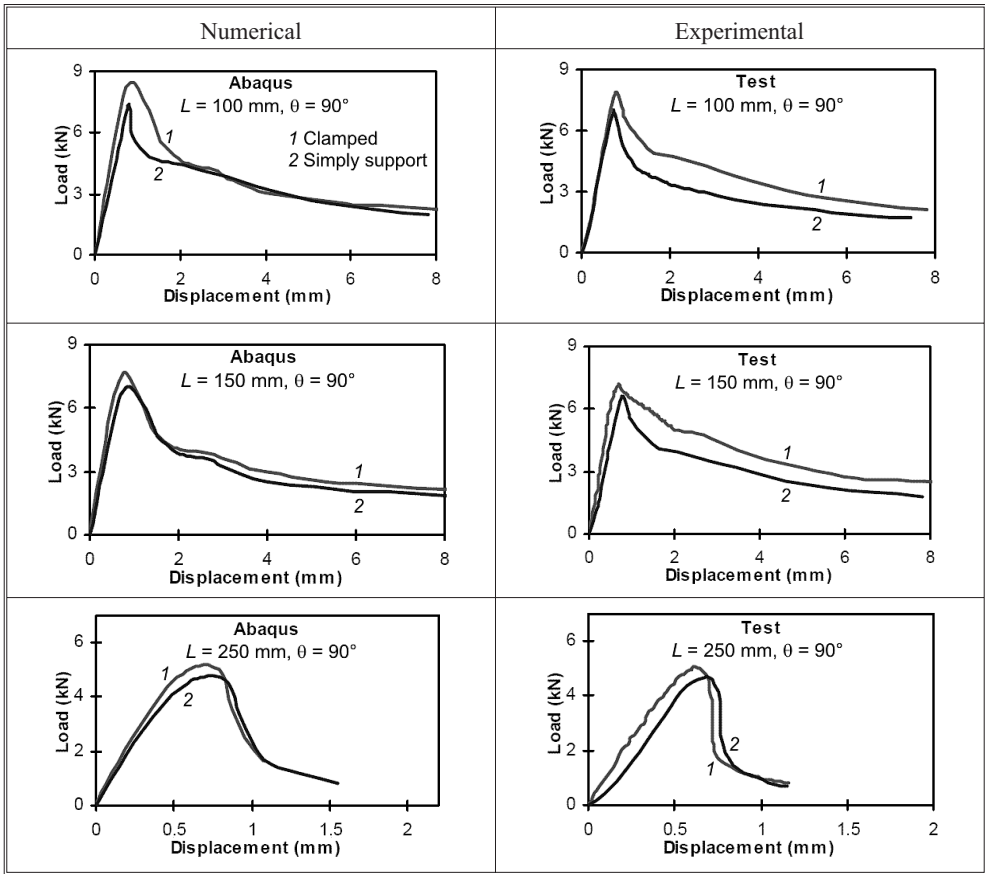
T a b l e 4

Buckling Load (kN) for Different Boundary Conditions

$\theta = 90°$	$L = 100$ mm		$L = 150$ mm		$L = 250$ mm	
	Numerical	Experimental	Numerical	Experimental	Numerical	Experimental
Simply supported	8.40	7.06	7.04	6.61	4.80	4.66
clamped	8.45	7.92	7.67	6.99	5.19	5.05

Fig. 15. Comparison of the experimental and numerical results.

T a b l e 5

Comparison of the Experimental and Numerical Results for Cylindrical Panels

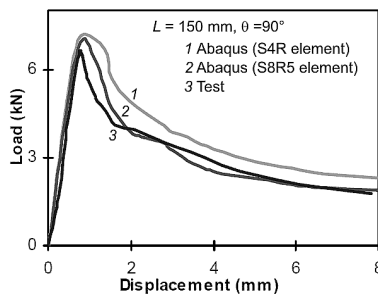| Model designation	Buckling load (kN)			Error (%)	
	S4R	S8R5	Experimental	S4R	S8R5
L100-θ90	7.541	7.410	7.060	6.8	4.8
L100-θ120	12.745	12.492	11.807	7.9	5.8
L100-θ180	16.124	16.027	15.021	7.3	6.7
L100-θ355	35.214	34.821	32.983	6.8	5.6
L100-perfect	43.245	43.038	40.934	5.6	5.1
L150-θ90	7.202	7.039	6.611	8.8	6.5
L150-θ120	11.459	11.265	11.048	3.7	2.0
L150-θ180	14.601	14.303	13.634	7.1	4.9
L150-θ355	32.249	31.029	29.652	8.7	4.6
L150-perfect	40.987	40.101	37.693	8.7	6.4
L250-θ90	4.912	4.802	4.659	5.4	3.1
L250-θ120	9.580	9.492	8.941	7.1	6.2
L250-θ180	13.375	13.345	12.596	6.2	5.9
L250-θ355	30.015	29.867	28.589	5.0	4.5
L250-perfect	38.012	37.436	36.223	4.9	3.4

Conclusions. Increase in the panel length decreases the buckling load. This effect is more critical for shorter panels. This can be attributed to the fact that the bending theory of shells is more suitable for lower t/L ratios, and this theory is used by the software for calculations.

The existence of a narrow slot decreases the buckling load noticeably.

The clamped boundary conditions increase the panel load-bearing capacity, i.e., increase the buckling load.

In the most cases, there is a good agreement between the numerical and experimental results. FE analysis results show that the curves constructed using linear elements predict the post-buckling region better than nonlinear elements, while the nonlinear elements are more suitable for calculation of the buckling load.

Р е з ю м е

Із використанням експериментальних і числових розрахункових методик досліджено поведінку циліндричних панелей після втрати стійкості. Проаналізовано вплив довжини, кутових параметрів секторів і різних граничних

умов циліндричних панелей на величину навантаження, за якого відбувається втрата стійкості. Експериментальні дослідження проводили на сервогідравлічній випробувальній машині Instron 8808, для розрахунків використовували скінченноелементний пакет програм Abaqus. Отримано хорошу збіжність розрахункових результатів з експериментальними.

1. M. Farshad, *Design and Analysis of Shell Structures*, Kluwer Academic Publishers, Dordrecht (1992).

2. B. Budiansky and J. W. Hutchinson (Eds.), *Buckling of Circular Cylindrical Shells under Axial Compression. Contributions to the Theory of Aircraft Structures*, Delft University Press (1972), pp. 239–260.

3. J. Arbocz and J. M. A. M. Hol, "Collapse of axially compressed cylindrical shells with random imperfections," *AIAA J.*, **29**, 2247–2256 (1991).

4. J. F. Jullien and A. Limam, "Effect of openings on the buckling of cylindrical shells subjected to axial compression," *Thin-Walled Struct.*, **31**, 187–202 (1998).

5. M. Farshad, *Stability of Structures*, Elsevier, Amsterdam (1994).

6. S. P. Timoshenko and J. M. Gere, *Theory of Elastic Stability*, McGraw-Hill, NewYork (1961).

7. S. G. Lekhnitskii, *Anisotropic Plates*, Gordon and Breach, New York (1968).

8. M. El-Raheb, "Response of a thin cylindrical panel with constrained edges," *Int. J. Solids Struct.*, **43**, 7571–7592 (2006).

9. K. Magnucki and M. Mackiewicz, "Elastic buckling of an axially compressed cylindrical panel with three edges simply supported and one edge free," *Thin-Walled Struct.*, **44**, 387–392 (2006).

10. S. N. Patel, P. K. Datta, and A. H. Sheikh, "Buckling and dynamic instability analysis of stiffened shell panels," *Thin-Walled Struct.*, **44**, 321–333 (2006).

11. P. Buermann, R. Rolfes, J. Tessmer, and M. Schagerl, "A semi-analytical model for local post-buckling analysis of stringer- and frame-stiffened cylindrical panels," *Thin-Walled Struct.*, **44**, 102–114 (2006).

12. L. Lanzi and V. Giavotto, "Post-buckling optimization of composite stiffened panels. Computations and experiments," *Compos. Struct.*, **73**, 208–220 (2006).

13. L. Jiang, Y. Wang, and X. Wang, "Buckling analysis of stiffened circular cylindrical panels using differential quadrature element method," *Thin-Walled Struct.*, **46**, 390–398 (2008).

14. C. Bisagni and R. Vescovini, "Analytical formulation for local buckling and post-buckling analysis of stiffened laminated panels," *Thin-Walled Struct.*, **47**, 318–334 (2009).

15. J. H. Kweon and C. S. Hong, "An improved arc-length method for post-buckling analysis of composite cylindrical panels," *Comp. Struct.*, **53**, No. 3, 541–549 (1994).

16. J. H. Kweon, "Post-failure analysis of composite cylindrical panels under compression," *J. Reinforced Plastics Composites*, **17**, No. 18, 1665–1681 (1998).

17. *ASTM A370-05. Standard Test Methods and Definitions for Mechanical Testing of Steel Products* (2005).

18. *ABAQUS 6.4 PR11 User's Manual*.

Received 04. 01. 2010